AGU Advances

RESEARCH ARTICLE
10.1029/2025AV001667

Remote Sensing Improves Multi-Hazard Flooding and Extreme Heat Detection by Fivefold Over Current Estimates

Matthew Preisser[1] **and Paola Passalacqua**[1]

[1]Fariborz Maseeh Department of Civil, Architectural, and Environmental Engineering, The University of Texas at Austin, Austin, TX, USA

Peer Review The peer review history for this article is available as a PDF in the Supporting Information.

Key Points:

- Methods for identifying flooding and heat hazards are not capturing the full extent that individuals are exposed to dangerous conditions
- We utilized a high-resolution satellite remote sensing methodology to increase the detection of flooding and heat events
- Increasing detection five-fold, we improve our ability to quantify how vulnerable populations are inequitably exposed to multi-hazards

Supporting Information:

Supporting Information may be found in the online version of this article.

Correspondence to:

P. Passalacqua and M. Preisser,
paola@austin.utexas.edu;
matthew.preisser@utexas.edu

Citation:

Preisser, M., & Passalacqua, P. (2025). Remote sensing improves multi-hazard flooding and extreme heat detection by fivefold over current estimates. *AGU Advances*, *6*, e2025AV001667. https://doi.org/10.1029/2025AV001667

Received 15 JAN 2025
Accepted 6 APR 2025

Author Contributions:

Conceptualization: Matthew Preisser, Paola Passalacqua
Data curation: Matthew Preisser
Formal analysis: Matthew Preisser, Paola Passalacqua
Funding acquisition: Matthew Preisser
Investigation: Matthew Preisser, Paola Passalacqua
Methodology: Matthew Preisser, Paola Passalacqua
Project administration: Matthew Preisser, Paola Passalacqua

Abstract

The co-occurrence of multiple hazards is of growing concern globally as the frequency and magnitude of extreme climate events increases. Despite studies examining the spatial distribution of such events, there has been little work in examining if all relevant life threatening and damaging hazards are captured in existing hazard databases and by common hazard metrics. For example, local/regional flash flooding events are seldom captured by optical satellite instruments and are subsequently excluded from global hazard databases. Similarly, the heat hazard definitions most frequently used in multi-hazard studies inherently fail to capture events that are life-threatening but climatologically within an expected range. Our goal is to determine the potential for increasing multi-hazard event detection capabilities by inferring additional hazard footprints from widely accessible satellite data. We use daily precipitation and temperature satellite data to develop an open-source framework that infers additional hazard footprints that are not included in traditional methods. With the state of Texas as our study area, we detected 2.5 times as many flood hazards, equivalent to $320 million in property and crop damages. Furthermore, our expanded heat hazard definition increases the impacted area by 56.6%, equivalent to 91.5 million km^2 over an 18 year period. Increasing hazard detection capabilities and expanding existing definitions of hazards using daily satellite data increases the temporal and spatial resolutions at which multi-hazard events are detected. Having more complete data sets of all relevant hazard extents improves our ability to track global trends and more accurately determine the magnitude of hazard exposure inequities.

Plain Language Summary

Expanding hazard detection capabilities is critical as climate extremes intensify. This study demonstrates the potential of daily satellite data to address limitations in current global hazard detection methods, which often exclude localized and life-threatening events like flash floods and extreme heat within expected climatological ranges. Using an open-source framework, we identified 2.5 times more flood events in Texas, equating to $320 million in damages, and increased the detected area of heat hazards by 56.6%, covering 91.5 million km^2 over 18 years. These advancements improve hazard monitoring, enabling more accurate assessments of climate risks and hazard exposure inequities. Enhanced detection of multi-hazard events supports better-informed responses to growing climate challenges worldwide.

1. Introduction

Climate change's threat to increasing future flood risks is well established, with current models suggesting damages will increase 10–20 fold in some locations over the next few decades (Hallegatte et al., 2013; Winsemius et al., 2015). Similar patterns of increased global risk exist for other hazards including droughts (Y. Liu & Chen, 2021), wildfires (Pausas & Keeley, 2021), and extreme heat events (Dong et al., 2015). In addition to climate change, anthropogenic factors (e.g., land use changes, floodplain management, impervious surface development, increased emissions, etc.) are increasing future flood and heat risks (Hounkpè et al., 2019; Kishore et al., 2022; Müller & Höfer, 2014; W. Zhang et al., 2022). These parallel trends in rising risks are just one component contributing to the increased interest in multi-hazard events. The United Nations (UN) and the Intergovernmental Panel on Climate Change (IPCC) define a hazard as a potentially damaging physical event that may cause loss of life, injury, property destruction, social/economic disruption or degradation (Cardona et al., 2012). Therefore, a multi-hazard event occurs when a hazard happens, simultaneously, cascadingly, or cumulatively (e.g., compounding) in time and space (UNDRR, 2016). While some studies specifically examine the mechanisms by which multi-hazard events influence each other (e.g., Gill & Malamud, 2014), in the context of this study a multi-hazard event is the occurrence of more than one hazard overlapping in time and space (e.g., Claassen et al., 2023; de Ruiter et al., 2020; Kappes et al., 2012).

Resources: Matthew Preisser
Software: Matthew Preisser
Supervision: Paola Passalacqua
Validation: Matthew Preisser
Visualization: Matthew Preisser
Writing – original draft: Matthew Preisser
Writing – review & editing: Matthew Preisser, Paola Passalacqua

Defining a multi-hazard event or identifying the appropriate modeling methodology can be a non-trivial task because of divergent methodologies of cross-disciplinary sciences (Kappes et al., 2012), the multitude of different compounding/cascading/triggering mechanisms (Tilloy et al., 2019), and the challenges associated with validating the accuracy of these relationships (Wang et al., 2020). While studies are beginning to identify some standardized approaches to creating coherent multi-hazard data sets (Claassen et al., 2023; Kappes et al., 2012), there remains a gap in addressing the completeness of the underlying input data into multi-hazard studies. We define *completeness* as the ability for an underlying hazard data set or definition to capture all relevant events that have an impact on society by imposing either physical damage or potentially life endangering situations. Flooding and extreme heat events, two of the most damaging natural hazards (Newman & Noy, 2023), are two event types whose completeness are particularly impacted by their input data.

In terms of flooding events, global multi-hazard research has predominantly relied on either hydrological models or flood databases. Studies that rely on hydrologically modeled information have the advantage of being able to incorporate future climate scenarios, which can greatly support the study of global hazard trends. However, limitations including coarser spatial resolutions, untested accuracy, high levels of uncertainty, and (sometimes) proprietary nature (e.g., Koks et al., 2019; Shi et al., 2015; Stalhandske et al., 2024) can make such models unsuitable for more regional analyses (Schubert et al., 2024; Ward et al., 2015). Databases have the advantage of being built on verifiable empirical evidence, reducing the uncertainty that may come from hydrological models. One of the leading global flood databases that continues to be utilized by researchers is the Dartmouth Flood Observatory (DFO) because it contains spatial data for over 4,900 events over 35 years (Brakenridge, 2024; Kettner et al., 2021). Entries in the database include a boundary shapefile showing the extent and location of the flooding event, and these boundaries directly supported the creation of the Global Flood Database (GFD), a collection of satellite derived flood extent maps that has increased our ability to detect exposed populations (Tellman et al., 2021). However, because specific criteria have to be met for an event to be considered large enough to be entered into the DFO, and specific conditions have to exist for satellite based delineation to be suitable (Notti et al., 2018; Tellman et al., 2021), there is a subset of flood hazard events not accounted for in the DFO or GFD databases.

Extreme heat is another common feature of many multi-hazard studies as a result of rising global temperatures and the threat of increased exposure to global populations (Forzieri et al., 2016). Most commonly, heat hazards are delineated using a *heatwave* definition, typically a minimum of three consecutive days where the temperature is above a defined percentile (e.g., 90th or 95th) for that location throughout the record length (Lavaysse et al., 2018; Nairn & Fawcett, 2014; Pezza et al., 2011; Ridder et al., 2020; C. Rogers et al., 2022; Sutanto et al., 2020). Analyzing temperature hazards through a heatwave metric alone fails to capture extreme temperatures that may be within climatologically expected ranges but are still detrimental to people and the environment (Bouchama et al., 2024). There are a few studies that alternatively focus on *heat events* through the number of days that exceed health standard thresholds (Heo et al., 2019; Stalhandske et al., 2024). Increases in the frequency and intensity of both heatwaves and heat events will increase the threat of heat-related illnesses on individuals, reduce ecosystem services, and decrease economic productivity (Margolis, 2020; Shayegh et al., 2020; Smale et al., 2019). However, the combination of both heatwave and heat event definitions in the same multi-hazard study is uncommon, and we are therefore likely undercounting the threat of rising global temperatures.

The goal of our work is to utilize high spatial and temporal resolution satellite remote sensing data to delineate flooding and extreme heat multi-hazard events and to determine if vulnerable populations are inequitably exposed. Here we present a framework for increasing our ability to delineate flooding and extreme heat multi-hazards and test it by observing events in Texas over the past two decades. We identify flood hazards as the regions where the sub-daily and multi-day precipitation average recurrence intervals (ARIs) are above a 2-year threshold. We verify the precipitation-based proxy flood hazard boundaries by comparing them to DFO events and the NOAA Storm Events Database. We identify heat hazards as the unary union of heatwaves and extreme heat events. We use a traditional 95th percentile heatwave metric definition and a heat wave metric based on the Wet Bulb Globe Temperature (WBGT) and occupational safety standards to identify when temperatures directly put people's health at risk as defined by recommended exposure limits (Anderson et al., 2013; Bernard & Iheanacho, 2015; Hawkins et al., 2016; Osczevski & Bluestein, 2005). The specifics of how flood and heat hazards are calculated can be found in the Methods section. Finally, we compare the extent to which existing methods (DFO boundaries and heatwaves, DFO/HW) and our expanded methods (ARI boundaries and merged heat events/waves, ARI/HH) can detect multi-hazard events across Texas, and we determine the impact of each set of methods on assessing hazard exposure inequities.

2. Methods

2.1. Texas and Extreme Weather Events

We chose Texas as our study area because it is one of the most impacted states in the United States in terms of extreme weather events. Of the 396 weather events in the United States that had a damage exceeding $1 billion (1980 through September 2024), Texas has been affected by the most of any state at 187 (47%, 58 more events than the next closest state), amounting to total damages between $300 and $430 billion from these storms alone (NCEI, 2024). Texas serves as an ideal case study region because of the frequency of extreme heat and flood events over the past 20 years, as well as it being the 2nd largest state in terms of population and area, having numerous diverse geographic and socioeconomic regions.

2.2. Existing Flood Hazard Databases

To determine the degree to which global databases are capturing all relevant flood hazard events, we compare the data record of the Dartmouth Flood Observatory (DFO) to the NOAA Storm Events Database between 2001 and 2020 (Brakenridge, 2024). The NOAA Storm Events Database was originally built to collect tornado event information (1950), was later expanded to include thunderstorm wind and hail event information (1955), and then transformed into a holistic database of 48 weather events (1996 to present). Events are entered based on reports from the National Weather Service's Weather Forecast Offices (NWS WFOs). An event's metadata typically include the event type (e.g., hail, flash flooding, thunderstorm wind, etc.), property/crop damage estimates, death/injury estimates, location attributes (state, county/NWS designated area, reporting WFO office), a narrative of the event, and often a geo-referenced point or line.

Events within the database are aggregated into *episodes*, which represent larger storm occurrences (e.g., multiple floods, damaging winds, and lightning strike events might make up a single storm episode over multiple days). We specifically filtered the database to only include the eight event types that directly relate to flooding: Coastal Flood, Flash Flood, Flood, Heavy Rain, Hurricane (Typhoon), Storm Surge/Tide, Tropical Depression and Tropical Storm. While the database captures a myriad of events and episodes, there are often multiple episodes that can be attributed to a single storm system as a result of either multiple WFOs not combining episodes across their reporting boundaries, or there being multiple days between event occurrences. For example, we estimate that Hurricane Harvey is a collection of at least 7 episodes, composed of 168 individual flood-related events when we compare the geographic and temporal distribution of database entries to the known extent and duration of the storm.

In order to capture the complete dynamics of storm systems for more accurate comparisons with other data sets, we cluster episodes into *storm periods*. A given storm period, p, is the union of a storm event, e, with all other storm events, e_i, out of the entire set, E, that are within a given distance, δ, and time, τ, from the first storm event (Equation 1).

$$p = e \cup \{e_i \in E \mid dist(e, e_i) \leq \delta \text{ and } \Delta t(e, e_i) \leq \tau\} \tag{1}$$

We set threshold values of 200-km and 3-day because they created the most coherent descriptions of known storm systems when we examined the geographic extent, temporal ranges, and event narratives of the combined episodes. We determined the geographic extent of each period based on the dissolved county boundaries of each event. While many event entries have other geographic information associated with them (e.g., begin/end coordinates, polylines, city locations), the precision and reporting frequency of these location attributes greatly impacted the accuracy of the delineated boundaries when solely relying on them, and therefore county boundaries produced the most consistent and logical footprints. Storm period metadata consist of the aggregated period and event metadata to capture the total estimated reported property/crop damages and deaths. Reported damage and death values are rough estimates, and WFOs take best efforts to update records as more information becomes available. To reduce the chances of erroneous NOAA database entries impacting defined storm periods, we apply a filter that removes any period that has less than two events (i.e., two positive confirmations an event actually occurred). We compare NOAA storm periods to DFO entries to determine the extent to which the DFO captures observed events, and we calculate what percentage of damages and deaths these storms account for.

2.3. Precipitation Based Proxy Flood Hazard Boundaries

We compare the combined microwave-infrared daily mean precipitation rate and the number of half-hourly precipitation retrievals (>0.01 mm/hr) from the Integrated Multi-satellitE Retrievals for Global Precipitation Measurement (IMERG) product (Final Run Level 3 data) with the gridded NOAA Atlas 14 Precipitation Frequency Estimates to compute the single day average recurrence intervals (ARIs) for every rainfall event (Huffman et al., 2023; Perica et al., 2018). A single day event, d, is the set of all cells, i,j, in the study area, $\mathbb{R}$, whose ARI value is greater than the designated threshold, α, and whose euclidian distance from another cell, $dist(i,j)$, is less than δ, or 200-km (Equation 2).

$$d = \{i,j \in \mathbb{R} | ARI_{i,j} \geq \alpha, \ \& \ \mathrm{dist}(i,j) \leq \delta\} \tag{2}$$

Similar to the aggregation method we utilized with the NOAA Storm Events Database, we merge multiple single day storm events together using the same spatial and temporal thresholds of 200-km and 3-day (Equation 1). If the new storm boundary is made of events that occur on multiple days, we calculate and threshold an additional event boundary (Equation 2), except that we utilize a multi-day ARI based on the sum of the total precipitation depth and total length in days of the event. Finally, we dissolve the daily and multi-day ARI storm episodes together to create the proxy boundaries and compare them against entries in the DFO and NOAA Storm Events Database to calculate the degree to which we can increase the detection of flood hazards.

It is important to note that precipitation is not the only driver of flood events, such as the case for storm surge and other coastal related flood events. However, all flood events within our study area contain a precipitation component and we can therefore identify regions that experienced some level of flooding due to the presence of high precipitation. Studies have shown significant dependence between rainfall and storm surge events (Zheng et al., 2013) as well as cyclones/hurricanes being the leading cause of compound flood events (Lai et al., 2021), which are the leading flood hazard source in terms of damages in our study area. We therefore rely on precipitation as our proxy flood hazard delineator.

We use a 2-year event as the ARI threshold (α) for what constitute a proxy flood hazard boundary. While a 2-year event may seem relatively low to what is typically considered a significant flood event (e.g., the 100- and 500-year event, or the 1% and 0.2% annual exceedance probability events) we have to consider the precipitation depths in the context of the daily time step and the available ARI data. For example, the Memorial Day Flood in Austin, Texas is often considered one of the worst recent flood events in the region and was driven by intense rainfall (Preisser et al., 2022). During this storm, a peak rainfall depth of 132-mm fell within five to six hours, while many surrounding areas registered between 80- and 90-mm of precipitation. Without considering the count of half-hourly observed precipitation intervals, 80-mm of rainfall in 24-hr is only a 1-year event for this area. When we do consider the count of observations to recognize the five to 6 hour storm length, the ARI rises to between a 2- and 5- year event. The NOAA Atlas 14 Precipitation Frequency Estimates publishes recurrence interval data for 1, 2, 5, 10, etc. year events. Upon examining known events (e.g., The Memorial Day Flood in Austin, TX, Hurricane Harvey, Texas May Floods, Tropical Storm Erin), we saw that 1-year events were not restrictive enough and 5-year events were too restrictive, resulting in our 2-year event threshold.

Examining half-hourly precipitation observations, 80% of the precipitation fell within two hours, raising the peak intensity to between a 25- and 50- year event. While sub-daily precipitation observations may better capture peak intensities, case-by-case knowledge of each event is required to define appropriate cumulative rainfall thresholds. Determining the exact intensity of rainfall events is not the goal of this work, rather we are interested in delineating generalized hazard boundary footprints and we therefore utilize the daily IMERG precipitation products. The daily precipitation product is the composite observation of the half-hourly measurements, and we therefore take advantage of the high temporal resolution of the underlying data while also benefiting from the generality that daily data provide. Furthermore, this flood event was a part of a month-long weather event throughout the entire state of Texas (Schumann et al., 2016), and including multi-day ARIs based on the total depth of water over the total number of days of the entire event captures the full extent of the hazard. Final event boundaries must also have a minimum area sum of 1,000 km^2 over the length of the event.

2.4. Heat Hazard Events

We calculate heat hazards (heatwaves and heat events) using a spatiotemporally filled daily minimum and maximum near-surface air temperature data set (2003–2020, 1-km) (T. Zhang et al., 2022). The global near-surface air temperature data set was derived from combining ground-station air temperature observations with satellite-based elevation and land surface temperature observations. Land surface temperature data come from the Moderate Resolution Imaging Spectroradiometer (MODIS) instruments aboard the Aqua and Terra satellites. We define a heatwave using the dominant existing method (e.g., Claassen et al., 2023; Pezza et al., 2011; C. Rogers et al., 2022). A location, i, is experiencing a heatwave, $w_i = 1$, at time t when there are a minimum of 3 consecutive days where both the minimum and maximum temperature, $T^{\min,\max}$, are above the 95th percentile, for that specific location, T_i^{95} (Equation 3). Additionally, we apply a 5-day moving window average to reduce the impact of outliers on the temperature record. Delineated heatwaves that have only one non-heatwave day between them are combined into single events.

$$w_i = \begin{cases} 1, & \text{if } \exists t \text{ s.t. } \sum_{k=0}^{2} 1\left(T_{i,t+k}^{\min,\max} > T_i^{95}\right) = 3 \\ 0, & \text{otherwise} \end{cases} \tag{3}$$

In terms of extreme heat events, air temperature alone is not enough to capture the complex relationships between human physiology and environmental thermal regulation (Basu & Samet, 2002; Kovats & Hajat, 2008; Leon, 2015; Mora et al., 2017). The wet bulb globe temperature (WBGT) accounts for additional meteorological variables (solar radiation, humidity, and wind speed) that influence the human impact of extreme temperatures, making it a more appropriate measurement for describing human-heat relationships (Bernard & Iheanacho, 2015). The WBGT is derived from a combination of three different types of thermometers: a black globe thermometer to determine the solar factor (sun angle and cloud coverage), a wet bulb thermometer to account for humidity, and a dry bulb thermometer for the ambient air temperature. Since the WBGT is not easily determined from satellite derived data sets because of the number of complex input variables, we utilize a surrogate relationship that only requires air temperature and relative humidity, or the heat index (Bernard & Iheanacho, 2015). We use the daily maximum near-surface air temperature (T, °F) along with daily relative humidity (R, percent) data to calculate the heat index (HI) and subsequently estimate the WBGT (°C) (Equations 4 and 5) (Bernard & Iheanacho, 2015). Daily global relative humidity data come from the Atmospheric Infrared Sounder instrument (AIRS Level 3) aboard the Aqua satellite (AIRS, 2019). To create a spatiotemporally filled data set, missing values are filled using a 5-day (5 days before and 5-day after) moving window average. If a location has more than 10 consecutive days without an observation, than the missing values are spatially interpolated by taking the average of the surrounding raster cells.

$$\begin{aligned} \text{Heat Index} = & -42.379 + 2.04901523T + 10.14333127R - 0.22475541TR \\ & -0.00683783T^2 - 0.05481717R^2 + 0.00122874T^2R \\ & +0.00085282TR^2 - 0.00000199T^2R^2 + \text{ADJ} \end{aligned} \tag{4}$$

where,

$$\text{ADJ} = \begin{cases} -\left(\dfrac{13-R}{4}\right)\cdot\sqrt{\dfrac{17-|T-95|}{17}}, & \text{if } R < 13\% \text{ and } 80°\text{F} \le T \le 112°\text{F}, \\ \left(\dfrac{R-85}{10}\right)\cdot\left(\dfrac{87-T}{5}\right), & \text{if } R > 85\% \text{ and } 80°\text{F} \le T \le 87°\text{F}, \\ 0, & \text{otherwise.} \end{cases} \tag{5}$$

The maximum WBGT recommended exposure limit thresholds from many major work place safety organizations including the Occupational Safety and Health Administration for light levels of work is 30°C (Jacklitsch et al., 2016). Light work is defined as standing, sitting, and moving objects less than 10 pounds. We use a threshold of 30°C based off of the daily maximum near-surface air temperature to align with daytime working conditions in order to discern when people's health is at risk of being negatively impacted. The delineated WBGT extreme heat hazards have the same three-consecutive day requirement as the heatwave calculation in order to reduce the impact of outlier single day extremes. The final heat hazard layer is the union of the calculated heatwave and heat event layers, relying on the same 200-km and 3-day aggregation parameters (Equation 1).

2.5. Multi-Hazard Events

We specifically focus on identifying situations where there is the potential for flooding and extreme heat events to compound, cascade, and/or trigger additional impacts, and are therefore interested in examining if vulnerable populations are exposed inequitably. Heat and flood hazards have vastly different spatial and temporal dynamics, and simply delineating a multi-hazard event as the co-occurrence of a heat and flood hazard may not capture the actual intensity of the event. For example, a flood that occurs in the middle of a month long versus a week long heatwave are two different kinds of multi-hazard events. We therefore calculate the number of multi-hazard *experiences*, which is the number of heat hazard days that occur within a given time-lag of each flood event. Time-lags in multi-hazard studies help capture when two different hazards overlap in space and occur within a given number of days of each other (Claassen et al., 2023; W. Zhang & Villarini, 2020). This approach is based on the idea that hazards can be described as a "space-time cube," where an event is a collection of overlapping gridded layers that capture the dynamics of a changing extent throughout both space and time. Our multi-hazard experiences definition is able to account for the durations of flood and heat events, and thus better captures exposure. We combine both the existing hazard definitions (DFO database and heatwaves, DFO/HW) and the proposed updated methodologies (ARI boundaries and merged heat events/waves, ARI/HH) into unique data sets to compare the differences in identifying multi-hazard experiences.

In order to identify if there are inequities in multi-hazard experience exposure, we calculate Lorenz curves, which are gaining renewed interest in various flood risk studies (Morgan, 1962; Preisser et al., 2023; Sanders et al., 2022). We use the vulnerability index developed by the Center for Disease Control (CDC) because it is readily available for the entire United States at the county level, the Census boundary most appropriate when considering the spatial resolution of the multi-hazards (Flanagan et al., 2011). We specifically examine the overall vulnerability index as well as the individual Socioeconomic Status, Household Characteristics, and Race & Ethnicity Status sub-metrics (Table S1). In order to compare both the differences in inequities and magnitude of multi-hazard experiences detected, we create generalized Lorenz curve plots, where instead of normalizing the y-axis to between 0 and 1, we plot the raw cumulative sum of multi-hazard experiences. Additionally, multi-hazard experiences are weighted by the population of each county to more accurately represent disparities in population exposure.

It is important to note that Lorenz curves measure equality, and in order to account for equity, vulnerability scores must be scaled to account for the difference in how impacts are felt (i.e., a more vulnerable county feels the impact of an event to a greater extent than a less vulnerable county experiencing the same exact impact). In order to scale the Lorenz curve to represent equity, every county's count of multi-hazard experiences is multiplied by an equally spaced value between 0 (least vulnerable) and n (most vulnerable), where n refers to the total number of counties (Preisser et al., 2023). To numerically represent inequities we also calculate Gini coefficients (measure of deviation from perfectly equitable society, where 0 is perfectly equitable and -1 and 1 are perfectly inequitable) and quarterly percent burdens (percent of cumulative sum of multi-hazard experiences encountered by each quarter of the population).

3. Results

3.1. Delineating Precipitation ARIs

For every rainfall event between 2001 and 2020, we compare daily precipitation (Figure 1a) and the count of half-hourly observations where rainfall exceeded a depth of 0.01 mm (Figure 1b) with NOAA precipitation frequency estimates. This comparison allows us to calculate the daily gridded ARI, which we threshold to a 2-year event to delineate likely flood hazard boundaries (Figure 1c). For example, the Memorial Day Flood in Austin, Texas (May 25th 2015) was a flash flood event that encompassed multiple counties as a result of rapid rainfall over a short period of time (Figure 1). While the storm system covered the majority of Texas, only a few counties experienced flood conditions as a result of rainfall on that day, which are appropriately identified using the daily ARI method (Figure 1c). In conjunction, we calculate a multi-day ARI for the duration of every precipitation event that lasts more than a single day to identify non-flash flood hazards (Figure 3b). The ARI method identified

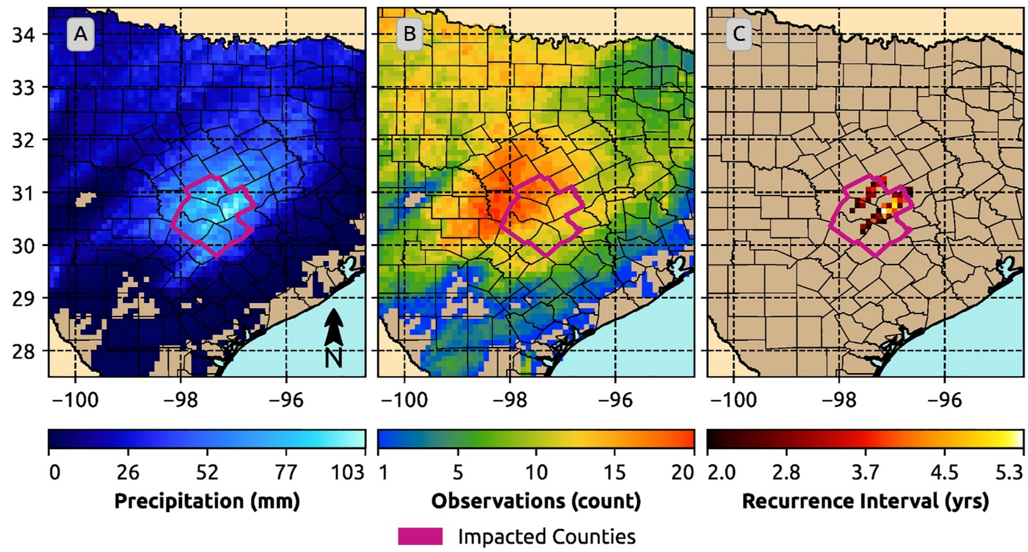

Figure 1. Example precipitation average recurrence interval (ARI) method for proxy flood hazard boundary delineation for May 25th 2015, showing (a) daily precipitation depth (mm), (b) the count of half hourly observations with more than 0.01 mm of precipitation, and (c) the average recurrence interval for rainfall.

a total of 190 potential flood hazard events between 2001 and 2020. 135 of these events can be validated when compared against the NOAA storm Events Database (Table 1). The 55 (28.9%) events that are potentially false positives might be explained through other hazards that are not directly related to flooding (e.g., extreme wind, lightning, hail).

3.2. Missing Flood Damages

Between 2001 and 2020, the NOAA Storm Events Database documented 9,388 flood-related events across 1,673 distinct episodes. We aggregated these episodes into 417 flood periods, having a total property and crop damage valuation of $76.1 billion (Table 1). The DFO has 53 entries that align with the delineated NOAA storm periods, accounting for only 12.7% of the events, but 99.2% and 80.1% of the damages and deaths, respectively. The ARI method produced 135 events that aligned with NOAA storm periods, 2.54 times as many as recorded in the DFO. Increasing event detection does not initially translate into a large difference in the damages and deaths being accounted for because of the positive skewness in the intensity of events. Nine storm periods encompass $74.1 billion of total damages, with Hurricane Harvey alone causing over $50 billion in damages. When excluding the nine most damaging storm periods, all of which individually caused over $700 million in damages, the detection capabilities drastically change for the DFO and ARI methods. While both data sets are still detecting relatively the same number of events as before, the ARI delineated events account for an additional $320 million in damages, a 23.2% difference compared to the DFO. Similar results exist in the number of recorded deaths, with the ARI method accounting for 26.3% more.

3.3. Spatial Comparison of Flood Boundaries

To test the effectiveness of the ARI method in creating comparable event extents, we compared ARI single- and multi-day delineations with the DFO and NOAA storm event database for multiple storm events (Figures 2 and 3). The 2015 May Floods, which encompassed the Memorial Day Flood (Figure 1), is often considered one of the worst statewide flood events in recent history, lasting for almost the entirety of the month of May and impacting the majority of the state (Figures 2a and 2b). The NOAA Storm Events Database and the DFO capture how the vast extent of the numerous floods that occurred. However, the DFO underestimates this extent, and fails to capture flood impacts in the southern half of the state (Figure 2c). On the other hand, the ARI method does a comparatively better job of identifying the hazard boundary (Figure 2d). Furthermore, this result highlights the usefulness of dual single and multi-day ARIs. The multi-day ARI method captures the true nature of the event,

Table 1
Dartmouth Flood Observatory (DFO) Flood Hazard Boundaries and Precipitation Average Recurrence Interval (ARI) Proxy Flood Hazard Boundary Cross Referenced With NOAA Storm Event Database Periods to Calculate the Sum of Events, Damages, and Deaths That Would Be Accounted for in Each Database Between 2001 and 2020

	All events			Events under $700M		
	Count	Damages ($Billions)	Deaths	Count	Damages ($Billions)	Deaths
NOAA	417	76.1	433	408	2.05	234
DFO	53 (12.7%)	75.5 (99.2%)	351 (80.1%)	44 (10.8%)	1.38 (67.3%)	152 (65.0%)
ARI	135 (32.3%)	75.8 (99.6%)	391 (90.3%)	126 (30.9%)	1.70 (82.9%)	192 (82.1%)

impacting the entire state over a longer time period, while the single-day ARI highlights some of the intense single day events that occurred during this time, such as the Memorial Day Flood in Austin.

We further examined and compared a number of other large flood events. Tropical Storm Erin is an example of where the ARI method and the DFO do not agree on the impacted area, although the ARI method better aligns with NOAA storm periods (Figure 3a). This difference could be a result of the DFO boundary being tied to the tropical storm track, which would have lost intensity as it moved inland. While the ARI method does under predict the impacted region, it is able to capture damaged areas outside of the direct tropical storm track. The Central Texas Floods were driven by the Brazos River flooding, which is captured in all of the databases to the eastern part of the state (Figure 3b). However, the DFO misses the other flood events that followed for the next month through Central Texas. The delineated hazard footprints for Hurricane Harvey generally align, showing the same impacted region (Figure 3c). The single day ARI method captures the majority of the full extent of the hurricane, with the multi-day ARI reconfirming the intensity of rainfall north of Houston, where the storm lagged before turning eastward. The 2018 June Flooding is the most expensive event not accounted for in the DFO, causing over $100 million in damages. The daily ARI shows substantial alignment when compared to the NOAA storm periods, and the multi-day ARI slightly over predicts the impacted extent (Figure 3d).

3.4. Increased Area Exposed to Extreme Heat

Between 2003 and 2020, there were 2,517 days (38.3% of all days) where a location in Texas was experiencing a heat hazard event. There was a total exposed area (i.e., the sum of areas experiencing a heat hazard over time) of 253.2 million km^2. Heatwaves and heat events identified the same heat hazard exposure area for 58.2 million km^2. Heatwaves and heat hazards individually accounted for 103.5 and 91.5 million km^2 of the impacted area, respectively. The addition of the heat events metric therefore increased the total impacted area by 56.6%.

August 9th, 2011 had the largest overlap between heatwaves and heat events and is one of the largest heat hazard days within Texas, being a part of the broader 2011 North American heatwave (Figure 4a). Heat hazard areas that overlap highlight how heatwaves and heat events are not mutually exclusive, suggesting that both are suitable for identifying similarly broad heat risks and there are likely many instances where heat hazards are a part of heatwaves. However, there are events where there is little to no agreement, such as June 27th, 2012 and July 7th, 2020, which were the largest heat event and heatwave days, respectively (Figures 4b and 4c). Annually, the addition of heat events regularly increases the total impacted area across Texas by relatively the same amount (Figure 4d).

3.5. Multi-Hazard Comparison

We compare the multi-hazard detection capabilities when using existing methods (DFO/HW) and our proposed expanded methods (ARI/HH) by calculating the number of *multi-hazard experiences*, or the number of days with a heat hazard within a given time lag around a flood event. Aggregating by county, regardless of time lag, the DFO/HW method detects multi-hazards primarily around the Gulf of Mexico, where most major flood events occur due to tropical weather (Figures 5a–5c). Comparatively, the ARI/HH method detects events throughout Texas, still covering the Gulf Coast region but also emphasizing events along the Texas-Mexico border, and throughout central Texas (Figures 5d–5f). There is a substantial difference in the magnitude of the number of multi-hazard experiences between the two methodologies. Across time-lags, the maximum number of multi-hazard experiences a county might encounter is approximately 5-times as more frequent when using the ARI/

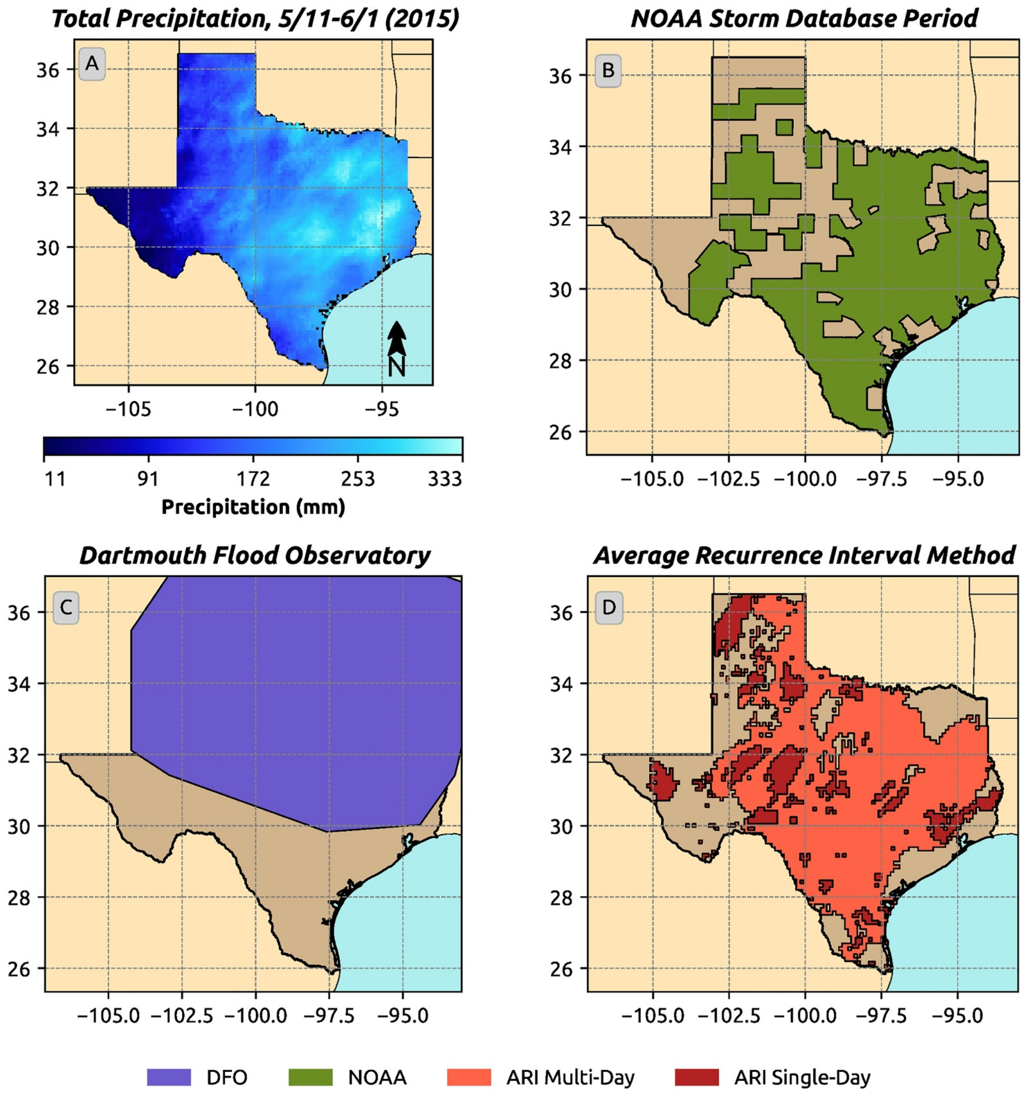

Figure 2. ARI method analysis for the 2015 May Floods, examining the total precipitation depth (a), the NOAA Storm Database periods (b), the Dartmouth Flood Observatory boundary (c), and the ARI method footprint (d).

HH methods. When examined annually, there are regularly more multi-hazard experiences when using the expanded ARI/HH methods (Figure 6). The last 6 years those data are available show some of the highest counts of multi-hazard experiences as a result of the increased occurrence of large scale heat hazards and major flooding events during these years.

Both DFO/HW and ARI/HH methods show substantial inequities across vulnerability indicators at the county level, as seen in all of the Gini coefficients being greater than 0 (Figure 7). Overall, the more vulnerable half of the population carries a much larger burden than the less vulnerable half of the population, with the DFO/HW and ARI/HH Q4 populations carrying on average 38% and 49% of the overall multi-hazard experience burden, respectively. In terms of the less vulnerable half of the population, there is little to no change from one indicator to the next on the burden that Q1 and Q2 carry, suggesting that exposure of hazards is only variable for the more vulnerable half of the population. Burdens increase for each quarter of the population across indicators, with the one exception of DFO/HW and Housing Characteristics, but this difference is small and still conveys that the burden is greater for the more vulnerable half of the population (Figure 7b). Race & Ethnicity have the greatest difference between the DFO/HW and ARI/HH methods, suggesting that a larger portion of the missed multi-hazard experiences are impacting minority counties (Figure 7c). Gini coefficients and burdens using the Socioeconomic and Overall Vulnerability indicators are nearly identical, suggesting that socioeconomic variables

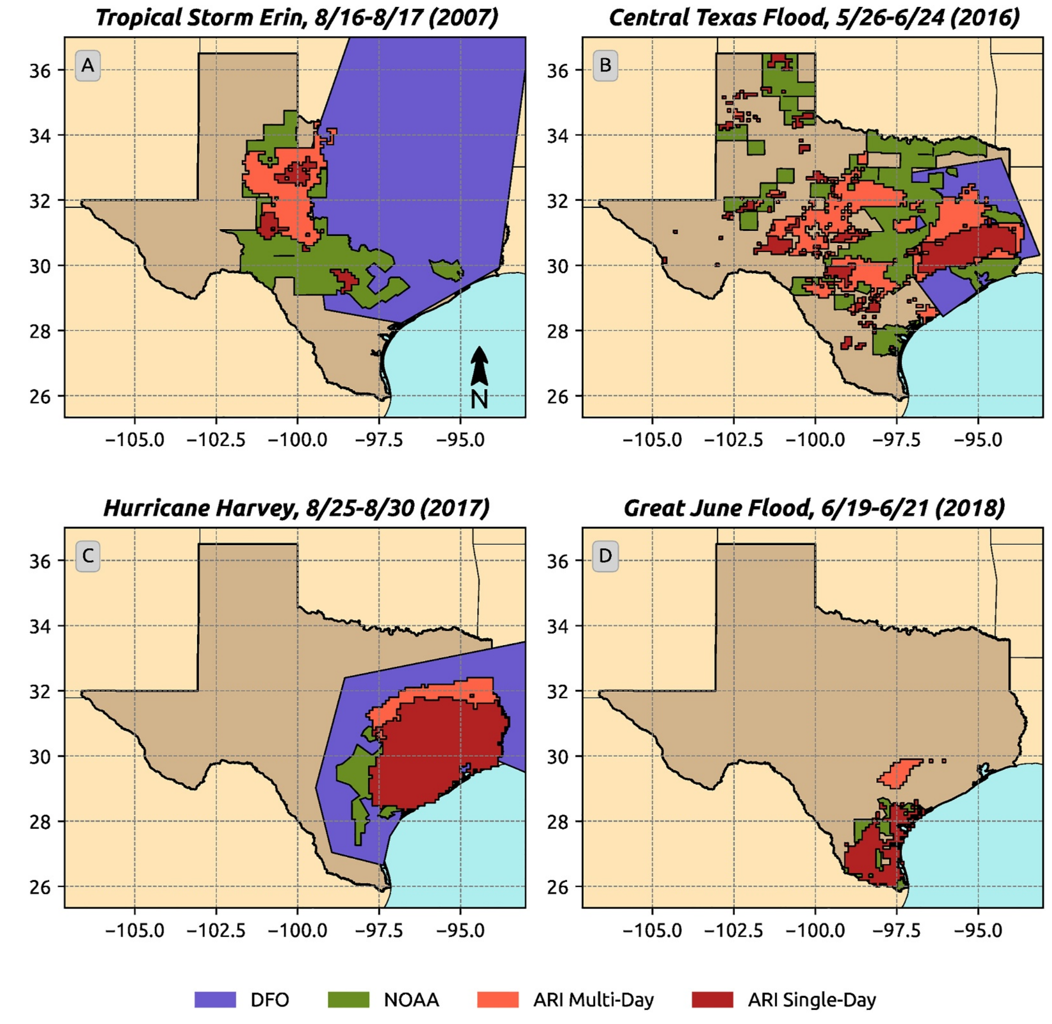

Figure 3. Comparison of Dartmouth Flood Observatory, ARI method, and NOAA storm periods flood hazard footprints for (a) Tropical Storm Erin, (b) the 2016 Central Texas floods, (c) Hurricane Harvey, and (d) the June 2018 floods.

are major predictors of this specific vulnerability indicator (Figures 7a and 7d). While both sets of methods show the same inequity trends, it is again further evident the degree to which the ARI/HH methods are detecting a greater amount of multi-hazard experiences.

4. Discussion

4.1. Flood Hazards

Climate models indicate that anthropogenic climate change is increasing the probability of intense rainfall events, which is directly related to increased rates of flood related damages (Davenport et al., 2021). Additionally, NOAA Atlas 14 data suggest that a greater proportion of the population is already exposed to higher extreme precipitation risk (Kim et al., 2023). Defining, identifying, and delineating extreme precipitation events, and subsequently flooding events, is therefore critical in order to describe their impacts on society (Gimeno et al., 2022). Although several databases exist—such as the International Disaster Database, the United Nations' ReliefWeb, and the International Flood Network—to document global floods, they often lack detailed information on the spatial and temporal extent of events or have limited historical records (Saharia et al., 2021). The DFO, a database that does meet many spatial and temporal requirements, is still missing events that cause hundreds of millions of dollars in damages, reveling that reliance on existing databases may be failing to capture the true increased extent in which global populations are exposed to flooding (Table 1).

10.1029/2025AV001667

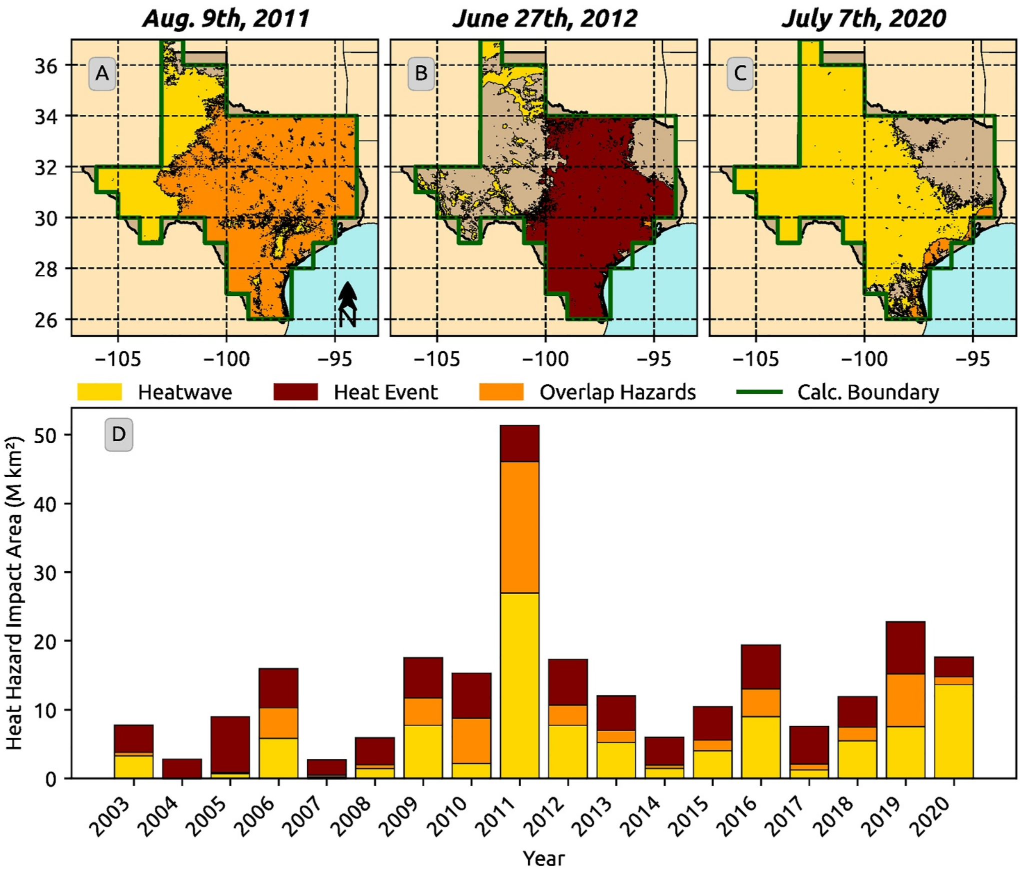

Figure 4. Example heat hazard (combination of 95th percentile heatwave and the 30°C wet bulb globe temperature heat event) delineations for (a) largest overlapping heatwave and heat event, (b) largest heat event (WBGT) day, and (c) largest heatwave (95th percentile) day. Annual sum of heatwave, heat event, and overlapping areas show degree to which heat events increase overall heat hazard area (d).

Our precipitation-based proxy flood hazard boundary method enhances detection capabilities by leveraging near-real-time precipitation data to identify likely damaged regions before formal damage assessments are completed. Large storm events that span entire states rarely cause damage uniformly, making it essential to have tools that pinpoint the most likely impacted areas (Figure 1). While not intended to replace flood mapping or modeling, our ARI method serves as a supplementary tool to support the maintenance of existing flood databases. It identified three times as many flood events as the DFO database, capturing an additional $320 million in damages (Table 1). The high agreement between ARI boundaries and the NOAA Storm Events Database further demonstrates the utility of the ARI method in identifying impacted areas in real time, increasing the proportion of damages accounted for in global flood databases (Figure 3).

At first glance, it appears that the ARI and DFO miss a substantial amount of hazards in the NOAA Storm Events Database, with over half of the total periods going unaccounted (Table 1). However, examining the matched and unmatched ARI-NOAA events, reveals that the unaccounted for events account for a small amount of impactful events. Of the unmatched NOAA storm periods, 25.8% report zero monetary damages, as compared to 11.1% of the matched events. Furthermore, the median damage for matched and unmatched events is $750,000 and $20,000 respectively, showing that the ARI method is capturing the majority of the high damage events. Finally, while we utilize a minimum two-event filter for NOAA storm periods, 86.9% of unmatched NOAA storm periods contained less than 10 events, compared to 20% of matched events. Taking all of this into consideration, the ARI method is identifying the vast majority of the damaging and large extent events, which is the most critical when identifying multi-hazard events.

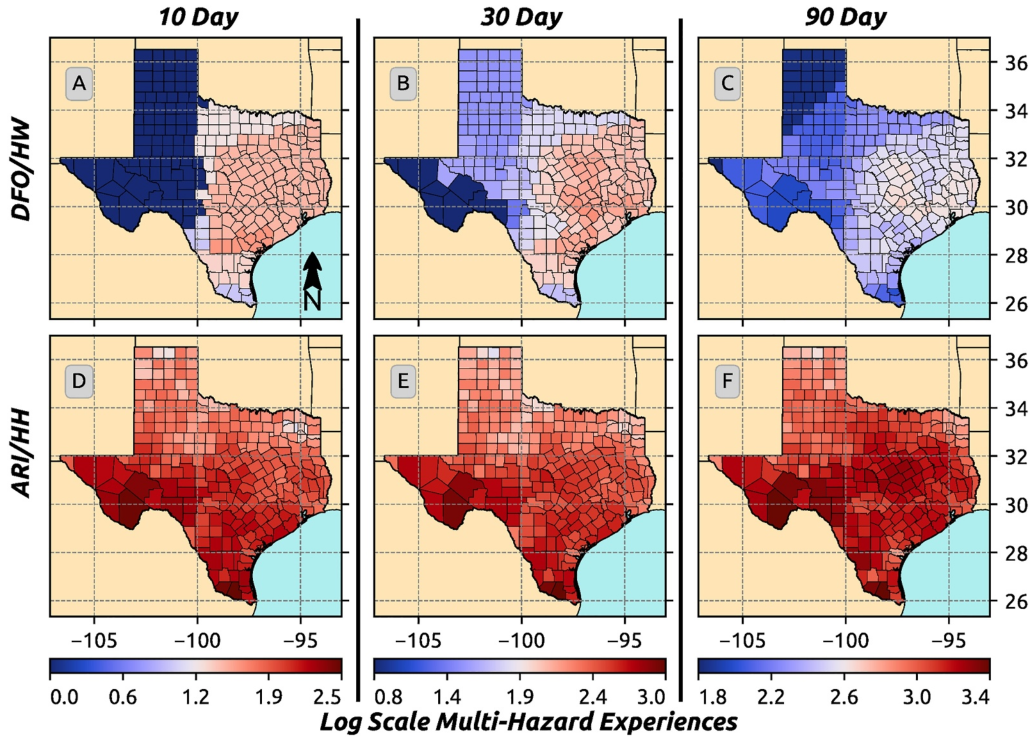

Figure 5. Log-scale multi-hazard experiences per county for the period 2003–2020 for the Dartmouth Flood Observatory and heatwave (DFO/HW) existing methods and the ARI and heat hazards (ARI/HH) expanded methods with a 10 (a, d), 30 (b, e), and 90 (c, f) day time-lags.

A limitation of this methodology is that extreme precipitation events do not always lead to flooding, or do not always lead to flooding that causes damages, as evident by the 55 false positive events. However, these events might be associated with other related multi-hazards, including storm events that produce damaging winds or hail. This limitation presents an opportunity to expand the ARI thresholding method to additional daily satellite remote sensing data sets to encompass more meteorological hazards. A key advantage of using a precipitation based metric to delineate potential flood hazards is that it is not constrained by traditional limitations of optical (spatial resolution, land use, cloud coverage) and radar (temporal resolution) based delineations of flooding (Notti et al., 2018). Existing precipitation based methods for early warning and near-real time flood detection are designed to be computationally lightweight in order to play a role in forecasting imminent hazards (e.g., Alfieri et al., 2011; Dao et al., 2020; Wu et al., 2012, 2014). We retain the advantages of low computational complexity and further benefit from not needing additional ground-based observations or coupling with hydrodynamic models.

4.2. Heat Hazards

It is estimated that nearly 48% of the global population will be exposed to extreme heat by the year 2100 (Mora et al., 2017). In terms of our study area, Texas has more heat-related worker deaths than any other state, and has set new state records for the number of overall heat-related deaths in 2021, 2022, and 2023 (Ball, 2024; Fauzia, 2024; Foxhill et al., 2024). Until recently, heat hazard research has predominantly focused on dry-heat events, undercounting the potential impacts of humidity and other climatic conditions on health risks (C. D. W. Rogers et al., 2021). The inclusion of additional climatic variables, such as through the use of the WBGT, has the advantage of being more closely tied to heat-related diseases (Heo et al., 2019). While there is an established lack of data related to the global risk of heat-related illnesses/mortality (Mora et al., 2017), the inclusion of extreme WBGT heat events directly enhances heat hazard identification practices through the inclusion of known worker safety standards (Jacklitsch et al., 2016).

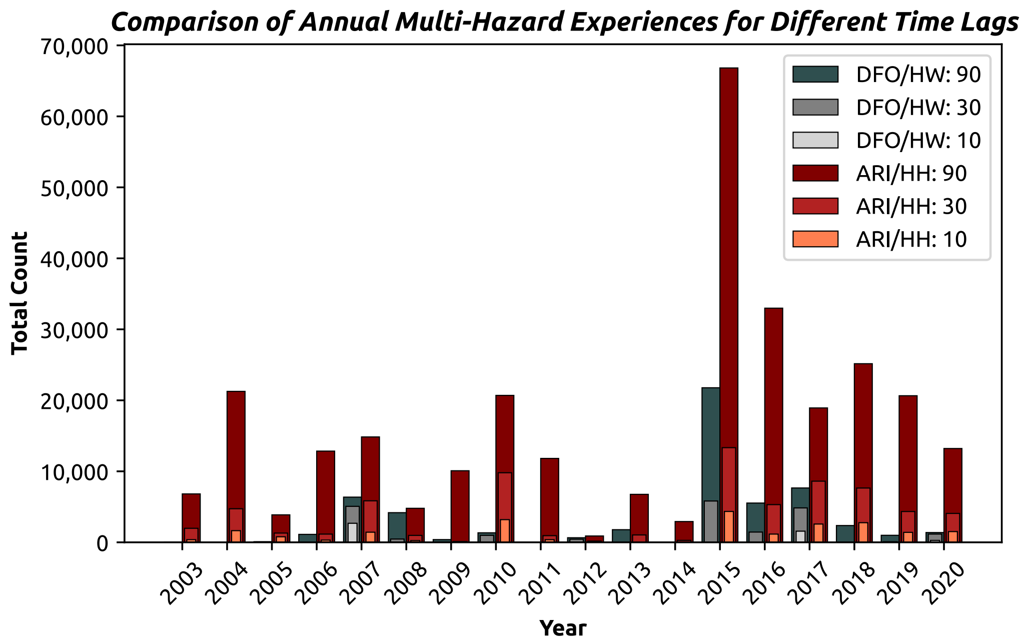

Figure 6. Annual multi-hazard experiences for the Dartmouth Flood Observatory and heatwave (DFO/HW) existing methods and the ARI and heat hazards (ARI/HH) expanded methods with a 10, 30, and 90 days time-lags.

The relatively similar annual increase in total impacted area as a result of the inclusion of WBGT is indicative of the two major limitations of the heatwave metric: first, the traditional heatwave metric does not account for the additional climatological conditions that humans experience. Second, temperatures under a 95th percentile threshold do not automatically guarantee safe working conditions 4D). The inclusion of WBGT heat events directly increases the duration and extent of heat hazard events, thus highlighting the importance of using dry- and wet-heat definitions when estimating heat exposure, especially for regions with the potential for high humidity. For example, when examining the location and extent of heat events within Texas, they are primarily located in the eastern half of the state, where humidity is higher as a result of there being more surface water and being closer to the Gulf of Mexico (Figures 4b and 4c). This condition coincides with the majority of population centers in Texas (e.g., Dallas, Austin, San Antonio, and Houston), all being more exposed to heat hazards when including additional relevant climatological information.

It is essential for multi-hazard studies to examine a combination of short- and long- term as well as dry- and wet-heat conditions to holistically capture how individuals are impacted in the context of their environments. We used a worker safety WBGT threshold of only 30°C, the occupational limit for light work, which does not encompass the vast majority of outdoor labor activities. We utilized a more strict heat event threshold to draw attention to the magnitude of how much a traditional heatwave definition is likely missing heat exposure. However, a daily 1-km analysis of hazards is going to inherently miss finer scale impacts of extreme heat (Kamath et al., 2023). Similar to our expanded flood delineation methods, our combined heatwave and heat event metric can be used to identify priority areas for more targeted and holistic heat hazard mitigations.

4.3. Multi-Hazards and Equity

Quantifying and analyzing the occurrence of multi-hazard events is of growing concern across disciplines as evident with the large number of review papers over the past few years (e.g., Drakes & Tate, 2022; Kappes et al., 2012; Leonard et al., 2013; Tilloy et al., 2019; Zscheischler et al., 2020), which is further supported by the increased number of multi-hazard experiences in the past 6 years (Figure 6). Flooding and extreme heat multi-hazard events can have specific triggering, intensifying, and compounding impacts on each other. For example, extreme heat events can influence local weather and increase the likelihood of flash flooding precipitation events (Chen et al., 2022; Fowler et al., 2021; W.Zhang & Villarini, 2020), heat events can lead to droughts which influence the intensity of flood events (Pizzorni et al., 2024), and flooding events can induce power outages making populations more susceptible to extreme heat events (Abi-Samra et al., 2014; Matthews et al., 2019). It is

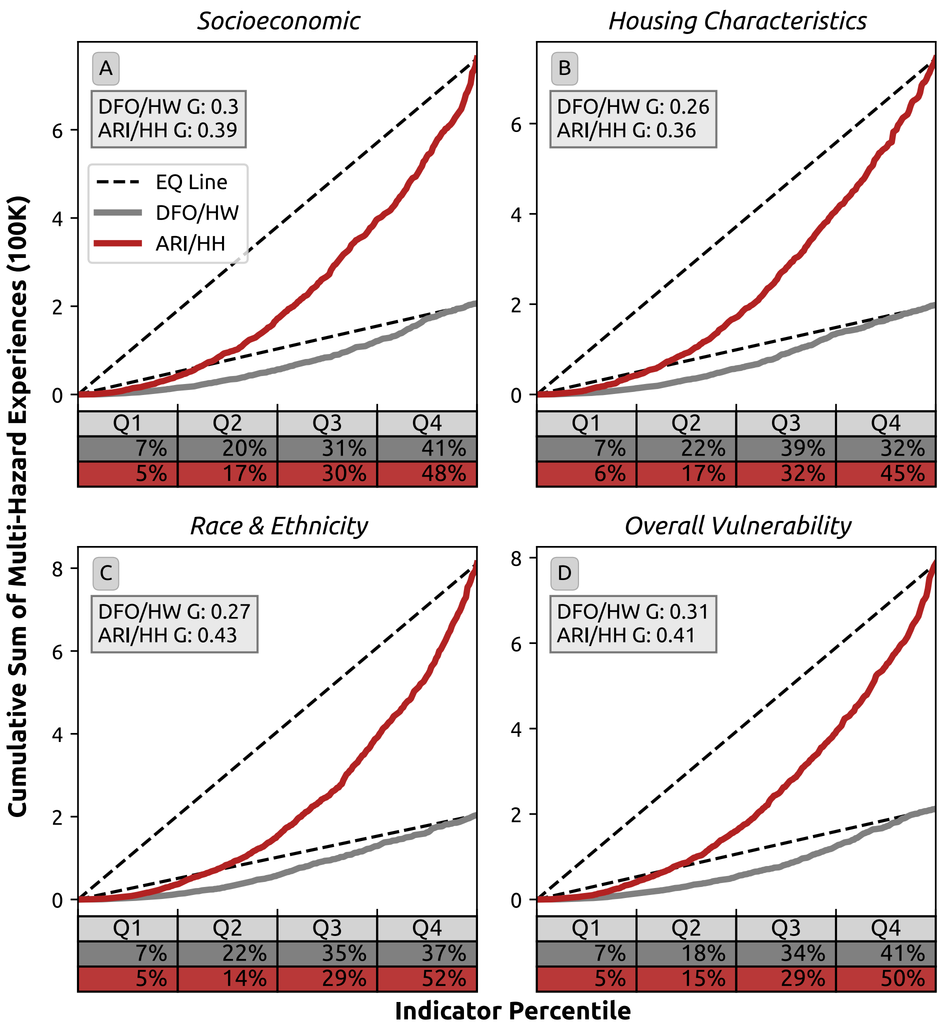

Figure 7. Generalized Lorenz curves of the Center for Disease Control's social vulnerability index versus the cumulative sum of multi-hazard experiences for the Dartmouth Flood Observatory and heatwave (DFO/HW) existing methods and the ARI and heat hazards (ARI/HH) expanded methods. 30 days time-lag county multi-hazard experience values are weighted by the logarithm of population to more accurately convey hazard exposure. Socioeconomic (a), Housing Characteristics (b), Race & Ethnicity (c), and overall Vulnerability (d) Gini coefficients and quarterly burdens are also presented.

also important to consider events that may not be individually extreme, as is the case for the 55 flood hazards that did not directly cause damage. For example, rainfall events followed by heatwaves can influence infectious disease outbreaks (McMichael, 2015).

The impact of multi-hazards on individuals is controlled by various variables including infrastructure capabilities, social and demographic characteristics, politics, finances, and culture (Barquet et al., 2023). In this study, we are specifically focusing on identifying the inequities in how different populations, defined by their sociodemographic vulnerability, are exposed to flooding and extreme heat multi-hazard events. Identifying the full extent of hazards and multi-hazards is critical in order to aid local, state, and national stakeholders in identifying priority areas of action when considering the limited resources available to address such issues. For example, as a part of the Texas State Flood Plan, managers identified over $54 billion worth of evaluations, projects, and management strategies that could reduce flood risk, but only a potential $10 billion in currently available funding (TWDB, 2024). Additionally, while heat risk perception may be growing in Texas, legislation to protect individuals may be lagging behind and more work is needed to identify priority mitigation locations (Dumlao & Debbage, 2023; Howe et al., 2019; Levitan, 2023; Mallen et al., 2019; Seong et al., 2022).

Comparing the locations of DFO/HW and ARI/HH delineated events with different time-lags highlights how existing methods might be failing to *completely* identify where multi-hazard events, or experiences, are occurring (Figure 5). With a 10-day time-lag, existing methods fail to identify any multi-hazards in the western half of the state, containing many counties with the highest level of exposure when using the updated ARI/HH methods (Figures 5a and 5c). While this problem begins to be alleviated with longer time-lags, it is still evident that the updated methods are detecting substantially more multi-hazards especially in southern and western counties. Many border counties have higher minority populations, contributing to larger differences in inequities when comparing the DFO/HW and ARI/HH methods using the Race & Ethnicity vulnerability indicator (Figure 7c). With studies showing that race and ethnicity variables can be related to a decrease in access to resources (e.g., Drakes & Tate, 2022; Preisser et al., 2023; Rufat et al., 2015), the under accounting of multi-hazard exposure based on the DFO/HW method could further perpetuate how minorities are marginalized by hazards.

Regardless of vulnerability metric and method, persistent inequities exist in multi-hazard experience exposure, with the ARI/HH method showing slightly more inequities across the board (Figure 7). In terms of future multi-hazard mitigation practices, perfect equity is not necessarily the goal. A hazard impacting a society equitably ($G = 0$) is less desirable than a hazard impacting only a handful of individuals ($G \neq 0$) (Logan et al., 2021). Identifying existing inequities is important for informing the decision making process so that resources can be distributed in an efficient and optimized manner. While our expanded methods do use the highest resolution (10-km precipitation and 1-km heat) available data sets, more targeted local studies are needed to more precisely identify effective mitigation strategies. Comparing multi-hazard events to county level social vulnerability estimates limits the spatial resolution at which inequities can be identified because of the heterogeneity that exists within counties. While tools and methods exist to estimate sociodemographic vulnerability at a higher resolution (e.g., Preisser et al., 2025), a finer examination is not currently possible because of the spatial limitations of using satellite data sets to define hazard events.

4.4. Scalability and Future Opportunities

We focused on Texas to highlight the multi-hazard risks in the state that is most impacted by climate hazards and contains four of the 10 most populated metropolitan areas in the United States (Houston, San Antonio, Dallas, and Austin). The benefit of utilizing satellite remote sensing data is their applicability to broad geographic regions that may not have local data sources. The only data source we used that is geographically bounded is the Atlas 14 Precipitation Frequencies (i.e., the annual recurrence interval information). Assuming similar data can be calculated based on global precipitation records, our proposed methods can be applied to the entire world, where there is a growing focus on identifying global multi-hazard events (Claassen et al., 2023). While the methods are directly transferable, local and regional knowledge will always be critical in identifying appropriate thresholds of what constitutes a hazard. For example, the relationship between precipitation and flooding will depend on a variety of local factors (e.g., design limits of flood infrastructure). Furthermore, what constitutes as a hazard in one location may not be a hazard in another. For example, acclimation can play a significant role when determining some levels of heat risk (Johnson et al., 2011). While our generalized approached can be appropriate in identifying broad multi-decadal trends in hazard exposure over broad regions, local action will require more nuanced examinations. There are additional opportunities to expand a satellite remote sensing multi-hazard delineation approach to additional hazards including extreme cold events, droughts, and non-meteorological hazards such as air quality (Forzieri et al., 2016; B. Liu et al., 2021; Salvo & Vitale, 2023).

4.5. Conclusion

Using Texas as our study area, we demonstrate that current methods for identifying hazards used in many multi-hazard analyses may underestimate both the frequency and geographic extent of events. This under-detection has serious implications for effective mitigation, leaving vulnerable populations, particularly marginalized communities, underprepared for life-threatening conditions. The proposed expanded methods, utilizing global precipitation and temperature data sets, increase our ability to detect flooding and extreme heat, accounting for a greater extent of the potential damaging and life threatening conditions that impact individuals. We found a five-fold increase in the number of multi-hazard events over a two decade period, composed of flood hazard events that caused over $300 million in damages and extreme heat events with a combined area of over 91.5 million km^2. Additional hazards can benefit from similar comparisons to empirical databases to verify their completeness, and future work is needed in identifying additional remotely sensed variables that are applicable for increasing hazard, and subsequently multi-hazard, detection capabilities. Relying on the extensive remote sensing global archive will allow researchers and practitioners to efficiently identify hazard footprints into the future as the network of Earth observing satellites continually grows. Significant work remains in the multi-hazard field in order to address challenges in forecasting future trends, creating better frameworks for risk management, and quantifying the feedbacks between hazards, exposure, and vulnerability (Ward et al., 2022).

Conflict of Interest

The authors declare no conflicts of interest relevant to this study.

Data Availability Statement

All data used in this study are freely and publicly available from their respective sources including the Dartmouth Flood Observatory (Brakenridge, 2024), the NOAA Storm Events Database (https://www.ncdc.noaa.gov/stormevents/), NOAA precipitation frequency estimates (Perica et al., 2018), GPM-IMERG precipitation data (Huffman et al., 2023), AIRS relative humidity data (AIRS, 2019), and the spatiotemporally filled near-surface air temperature data set (T. Zhang et al., 2022). The code used in this study can be found at (Preisser & Passalacqua, 2025).

Acknowledgments

This work was supported by the National Science Foundation Graduate Research Fellowship (NSFGRFP, Grant DGE-1610403), the Future Investigators in NASA Earth and Space Science and Technology (NASA FINESST, Grant 21-EARTH21-0264), Planet Texas 2050, a research grand challenge at the University of Texas at Austin, and the U.S. Department of Energy, Office of Science, Biological and Environmental Research Program's Southeast Texas Urban Integrated Field Laboratory under Award Number DE-SC0023216.

References

Abi-Samra, N., McConnach, J., Mukhopadhyay, S., & Wojszczyk, B. (2014). When the bough breaks: Managing extreme weather events affecting electrical power grids. *IEEE Power and Energy Magazine*, *12*(5), 61–65. https://doi.org/10.1109/mpe.2014.2331899

AIRS. (2019). Aqua/AIRS L3 daily standard physical retrieval (AIRS-only) 1 degree x 1 degree v7.0 [Dataset]. *AIRS*. https://doi.org/10.5067/UO3Q64CTTS1U

Alfieri, L., Velasco, D., & Thielen, J. (2011). Flash flood detection through a multi-stage probabilistic warning system for heavy precipitation events. *Advances in Geosciences*, *29*, 69–75. https://doi.org/10.5194/adgeo-29-69-2011

Anderson, G. B., Bell, M. L., & Peng, R. D. (2013). Methods to calculate the heat index as an exposure metric in environmental health research. *Environmental Health Perspectives*, *121*(10), 1111–1119. https://doi.org/10.1289/ehp.1206273

Ball, A. (2024). Hostage to heat: Worked to death. Retrieved from https://stories.usatodaynetwork.com/hostagetoheat/texas-heat-no-regulations-cause-workers-death/

Barquet, K., Englund, M., Inga, K., André, K., & Segnestam, L. (2023). Conceptualising multiple hazards and cascading effects on critical infrastructures. *Disasters*, *48*(1). https://doi.org/10.1111/disa.12591

Basu, R., & Samet, J. (2002). Relation between elevated ambient temperature and mortality: A review of the epidemiologic evidence. *Epidemiologic Reviews*, *24*(2), 190–202. https://doi.org/10.1093/epirev/mxf007

Bernard, T. E., & Iheanacho, I. (2015). Heat index and adjusted temperature as surrogates for wet bulb globe temperature to screen for occupational heat stress. *Journal of Occupational and Environmental Hygiene*, *12*(5), 323–333. https://doi.org/10.1080/15459624.2014.989365

Bouchama, A., Mündel, T., & Laitano, O. (2024). Beyond heatwaves: A nuanced view of temperature-related mortality. *Temperature*, 1–13. https://doi.org/10.1080/23328940.2024.2310459

Brakenridge, G. (2024). Global active archive of large flood events [Dataset]. *Dartmouth Flood Observatory, University of Colorado*. Retrieved from http://floodobservatory.colorado.edu/Archives/

Cardona, O.-D., van Aalst, M. K., Birkmann, J., Fordham, M., McGregor, G., Perez, R., et al. (2012). Determinants of risk: Exposure and vulnerability. In *Managing the risks of extreme events and disasters to advance climate change adaptation* (pp. 65–108). Cambridge University Press. https://doi.org/10.1017/cbo9781139177245.005

Chen, Y., Liao, Z., Shi, Y., Li, P., & Zhai, P. (2022). Greater flash flood risks from hourly precipitation extremes preconditioned by heatwaves in the Yangtze River valley. *Geophysical Research Letters*, *49*(18), e2022GL099485. https://doi.org/10.1029/2022gl099485

Claassen, J. N., Ward, P. J., Daniell, J., Koks, E. E., Tiggeloven, T., & de Ruiter, M. C. (2023). A new method to compile global multi-hazard event sets. *Scientific Reports*, *13*(1), 13808. https://doi.org/10.1038/s41598-023-40400-5

Dao, D. A., Kim, D., Park, J., & Kim, T. (2020). Precipitation threshold for urban flood warning—An analysis using the satellite-based flooded area and radar-gauge composite rainfall data. *Journal of Hydro-environment Research*, *32*, 48–61. https://doi.org/10.1016/j.jher.2020.08.001

Davenport, F. V., Burke, M., & Diffenbaugh, N. S. (2021). Contribution of historical precipitation change to us flood damages. *Proceedings of the National Academy of Sciences of the United States of America*, *118*(4). https://doi.org/10.1073/pnas.2017524118

de Ruiter, M. C., Couasnon, A., van den Homberg, M. J. C., Daniell, J. E., Gill, J. C., & Ward, P. J. (2020). Why we can no longer ignore consecutive disasters. *Earth's Future*, *8*(3). https://doi.org/10.1029/2019ef001425

Dong, W., Liu, Z., Liao, H., Tang, Q., & Li, X. (2015). New climate and socio-economic scenarios for assessing global human health challenges due to heat risk. *Climatic Change*, *130*(4), 505–518. https://doi.org/10.1007/s10584-015-1372-8

Drakes, O., & Tate, E. (2022). Social vulnerability in a multi-hazard context: A systematic review. *Environmental Research Letters*, *17*(3), 033001. https://doi.org/10.1088/1748-9326/ac5140

Dumlao, A., & Debbage, N. (2023). Examining the spatial proximity of vulnerable communities to cooling centers across the Texas triangle megaregion. *Weather, Climate, and Society*, *15*(4), 1085–1098. https://doi.org/10.1175/wcas-d-22-0125.1

Fauzia, M. (2024). Annual heat-related deaths in Texas have tripled since 2018 here's how to stay hydrated. Retrieved from https://www.dallasnews.com/news/2024/08/12/annual-heat-related-deaths-in-texas-have-tripled-since-2018-heres-how-to-stay-hydrated/

Flanagan, B. E., Gregory, E. W., Hallisey, E. J., Heitgerd, J. L., & Lewis, B. (2011). A social vulnerability index for disaster management. *Journal of Homeland Security and Emergency Management*, *8*(1). https://doi.org/10.2202/1547-7355.1792

Forzieri, G., Feyen, L., Russo, S., Vousdoukas, M., Alfieri, L., Outten, S., et al. (2016). Multi-hazard assessment in Europe under climate change. *Climatic Change*, *137*(1–2), 105–119. https://doi.org/10.1007/s10584-016-1661-x

Fowler, H. J., Lenderink, G., Prein, A. F., Westra, S., Allan, R. P., Ban, N., et al. (2021). Anthropogenic intensification of short-duration rainfall extremes. *Nature Reviews Earth & Environment*, *2*(2), 107–122. https://doi.org/10.1038/s43017-020-00128-6

Foxhill, E., Martinex, A., Schumacher, Y., Baddour, D., & Pskowski, M. (2024). Texas likely undercounting heat-related deaths. Retrieved from https://www.texastribune.org/2024/08/14/texas-heat-deaths-undercount

Gill, J. C., & Malamud, B. D. (2014). Reviewing and visualizing the interactions of natural hazards: Interactions of natural hazards. *Reviews of Geophysics*, *52*(4), 680–722. https://doi.org/10.1002/2013rg000445

Gimeno, L., Sorí, R., Vázquez, M., Stojanovic, M., Algarra, I., Eiras-Barca, J., et al. (2022). Extreme precipitation events. *WIREs Water*, *9*(6). https://doi.org/10.1002/wat2.1611

Hallegatte, S., Green, C., Nicholls, R. J., & Corfee-Morlot, J. (2013). Future flood losses in major coastal cities. *Nature Climate Change*, *3*(9), 802–806. https://doi.org/10.1038/nclimate1979

Hawkins, M. D., Brown, V., & Ferrell, J. (2016). Assessment of NOAA national weather service methods to warn for extreme heat events. *Weather, Climate, and Society*, *9*(1), 5–13. https://doi.org/10.1175/wcas-d-15-0037.1

Heo, S., Bell, M. L., & Lee, J.-T. (2019). Comparison of health risks by heat wave definition: Applicability of wet-bulb globe temperature for heat wave criteria. *Environmental Research*, *168*, 158–170. https://doi.org/10.1016/j.envres.2018.09.032

Hounkpè, J., Diekkrüger, B., Afouda, A. A., & Sintondji, L. O. C. (2019). Land use change increases flood hazard: A multi-modelling approach to assess change in flood characteristics driven by socio-economic land use change scenarios. *Natural Hazards*, *98*(3), 1021–1050. https://doi.org/10.1007/s11069-018-3557-8

Howe, P. D., Marlon, J. R., Wang, X., & Leiserowitz, A. (2019). Public perceptions of the health risks of extreme heat across us states, counties, and neighborhoods. *Proceedings of the National Academy of Sciences of the United States of America*, *116*(14), 6743–6748. https://doi.org/10.1073/pnas.1813145116

Huffman, G., Stocker, E., Bolvin, D., Nelkin, E., & Tan, J. (2023). GPM IMERG final precipitation l3 1 day 0.1 degree x 0.1 degree v07 [Dataset]. https://doi.org/10.5067/GPM/IMERGDF/DAY/07

Jacklitsch, B. L., Williams, W. J., Musolin, K., Coca, A., Kim, J.-H., & Turner, N. (2016). Occupational exposure to heat and hot environments: Revised criteria 2016. Retrieved from https://www.cdc.gov/niosh/docs/2016-106/

Johnson, D., Lulla, V., Stanforth, A., & Webber, J. (2011). Remote sensing of heat-related health risks: The trend toward coupling socioeconomic and remotely sensed data: Remote sensing of heat-related health risks. *Geography Compass*, *5*(10), 767–780. https://doi.org/10.1111/j.1749-8198.2011.00442.x

Kamath, H. G., Martilli, A., Singh, M., Brooks, T., Lanza, K., Bixler, R. P., et al. (2023). Human heat health index (h3i) for holistic assessment of heat hazard and mitigation strategies beyond urban heat islands. *Urban Climate*, *52*, 101675. https://doi.org/10.1016/j.uclim.2023.101675

Kappes, M. S., Keiler, M., von Elverfeldt, K., & Glade, T. (2012). Challenges of analyzing multi-hazard risk: A review. *Natural Hazards*, *64*(2), 1925–1958. https://doi.org/10.1007/s11069-012-0294-2

Kettner, A., Brakenridge, G. R., Schumann, G. J.-P., & Shen, X. (2021). Dfo—Flood observatory. In *Earth observation for flood applications* (pp. 147–164). Elsevier. https://doi.org/10.1016/b978-0-12-819412-6.00007-9

Kim, J., Porter, J., & Kearns, E. J. (2023). Exposure of the US population to extreme precipitation risk has increased due to climate change. *Scientific Reports*, *13*(1), 21782. https://doi.org/10.1038/s41598-023-48969-7

Kishore, P., Basha, G., Venkat Ratnam, M., AghaKouchak, A., Sun, Q., Velicogna, I., & Ouarda, T. B. J. M. (2022). Anthropogenic influence on the changing risk of heat waves over India. *Scientific Reports*, *12*(1), 3337. https://doi.org/10.1038/s41598-022-07373-3

Koks, E. E., Rozenberg, J., Zorn, C., Tariverdi, M., Vousdoukas, M., Fraser, S. A., et al. (2019). A global multi-hazard risk analysis of road and railway infrastructure assets. *Nature Communications*, *10*(1), 2677. https://doi.org/10.1038/s41467-019-10442-3

Kovats, R. S., & Hajat, S. (2008). Heat stress and public health: A critical review. *Annual Review of Public Health*, *29*(1), 41–55. https://doi.org/10.1146/annurev.publhealth.29.020907.090843

Lai, Y., Li, J., Gu, X., Liu, C., & Chen, Y. D. (2021). Global compound floods from precipitation and storm surge: Hazards and the roles of cyclones. *Journal of Climate*, 1–55. https://doi.org/10.1175/jcli-d-21-0050.1

Lavaysse, C., Cammalleri, C., Dosio, A., van der Schrier, G., Toreti, A., & Vogt, J. (2018). Towards a monitoring system of temperature extremes in Europe. *Natural Hazards and Earth System Sciences*, *18*(1), 91–104. https://doi.org/10.5194/nhess-18-91-2018

Leon, L. R. (2015). Pathophysiology of heat stroke. *Colloquium Series on Integrated Systems Physiology: From Molecule to Function*, *7*(2), 1–101. https://doi.org/10.4199/c00128ed1v01y201503isp060

Leonard, M., Westra, S., Phatak, A., Lambert, M., van den Hurk, B., McInnes, K., et al. (2013). A compound event framework for understanding extreme impacts. *WIREs Climate Change*, *5*(1), 113–128. https://doi.org/10.1002/wcc.252

Levitan, H. (2023). Amid a record heat wave, Texas construction workers lose their right to rest breaks. Retrieved from https://www.npr.org/sections/health-shots/2023/07/21/1189179220/amid-a-record-heat-wave-texas-construction-workers-lose-their-right-to-rest-brea

Liu, B., Han, X., Qin, L., Xu, W., & Fan, J. (2021). Multi-hazard risk mapping for coupling of natural and technological hazards. *Geomatics, Natural Hazards and Risk*, *12*(1), 2544–2560. https://doi.org/10.1080/19475705.2021.1969451

Liu, Y., & Chen, J. (2021). Future global socioeconomic risk to droughts based on estimates of hazard, exposure, and vulnerability in a changing climate. *Science of the Total Environment*, *751*, 142159. https://doi.org/10.1016/j.scitotenv.2020.142159

Logan, T., Anderson, M., Williams, T., & Conrow, L. (2021). Measuring inequalities in urban systems: An approach for evaluating the distribution of amenities and burdens. *Computers, Environment and Urban Systems*, *86*, 101590. https://doi.org/10.1016/j.compenvurbsys.2020.101590

Mallen, E., Stone, B., & Lanza, K. (2019). A methodological assessment of extreme heat mortality modeling and heat vulnerability mapping in Dallas, Texas. *Urban Climate*, *30*, 100528. https://doi.org/10.1016/j.uclim.2019.100528

Margolis, H. G. (2020). Heat waves and rising temperatures: Human health impacts and the determinants of vulnerability. In *Respiratory medicine* (pp. 123–161). Springer International Publishing. https://doi.org/10.1007/978-3-030-54746-2_7

Matthews, T., Wilby, R. L., & Murphy, C. (2019). An emerging tropical cyclone–deadly heat compound hazard. *Nature Climate Change*, *9*(8), 602–606. https://doi.org/10.1038/s41558-019-0525-6

McMichael, A. J. (2015). Extreme weather events and infectious disease outbreaks. *Virulence*, *6*(6), 543–547. https://doi.org/10.4161/21505594.2014.975022

Mora, C., Dousset, B., Caldwell, I. R., Powell, F. E., Geronimo, R. C., Bielecki, C., et al. (2017). Global risk of deadly heat. *Nature Climate Change*, *7*(7), 501–506. https://doi.org/10.1038/nclimate3322

Morgan, J. (1962). The anatomy of income distribution. *The Review of Economics and Statistics*, *44*(3), 270. https://doi.org/10.2307/1926398

Müller, A., & Höfer, R. (2014). The impacts of climate and land-use change on flood and heat hazards. In *Climate adaptation santiago* (pp. 107–126). Springer Berlin Heidelberg. https://doi.org/10.1007/978-3-642-39103-3_6

Nairn, J., & Fawcett, R. (2014). The excess heat factor: A metric for heatwave intensity and its use in classifying heatwave severity. *International Journal of Environmental Research and Public Health*, *12*(1), 227–253. https://doi.org/10.3390/ijerph120100227

NCEI. (2024). US billion-dollar weather and climate disasters. https://doi.org/10.25921/stkw-7w73

Newman, R., & Noy, I. (2023). The global costs of extreme weather that are attributable to climate change. *Nature Communications*, *14*(1), 6103. https://doi.org/10.1038/s41467-023-41888-1

Notti, D., Giordan, D., Caló, F., Pepe, A., Zucca, F., & Galve, J. (2018). Potential and limitations of open satellite data for flood mapping. *Remote Sensing*, *10*(11), 1673. https://doi.org/10.3390/rs10111673

Osczevski, R., & Bluestein, M. (2005). The new wind chill equivalent temperature chart. *Bulletin of the American Meteorological Society*, *86*(10), 1453–1458. https://doi.org/10.1175/bams-86-10-1453

Pausas, J. G., & Keeley, J. E. (2021). Wildfires and global change. *Frontiers in Ecology and the Environment*, *19*(7), 387–395. https://doi.org/10.1002/fee.2359

Perica, S., Pavlovic, S., Laurent, M. S., Trypaluk, C., Unruh, D., & Wilhite, O. (2018). NOAA atlas 14 volume 11 version 2, precipitation-frequency atlas of the United States, Texas (Tech. Rep.). https://doi.org/10.25923/1ceg-5094

Pezza, A. B., van Rensch, P., & Cai, W. (2011). Severe heat waves in southern Australia: Synoptic climatology and large scale connections. *Climate Dynamics*, *38*(1–2), 209–224. https://doi.org/10.1007/s00382-011-1016-2

Pizzorni, M., Innocenti, A., & Tollin, N. (2024). Droughts and floods in a changing climate and implications for multi-hazard urban planning: A review. *City and Environment Interactions*, *24*, 100169. https://doi.org/10.1016/j.cacint.2024.100169

Preisser, M., & Passalacqua, P. (2025). Software for "remote sensing improves multi-hazard flooding and extreme heat detection by fivefold over current estimates" [Dataset]. *Zenodo*. Retrieved from https://zenodo.org/records/15178573

Preisser, M., Passalacqua, P., & Bixler, R. P. (2025). Svinsight (1.2): A python package for calculating social vulnerability indices [Dataset]. *[Zenodo Repository]*. Retrieved from https://github.com/mdp0023/SVInsight

Preisser, M., Passalacqua, P., Bixler, R. P., & Boyles, S. (2023). A network-based analysis of critical resource accessibility during floods. *Frontiers in Water*, *5*. https://doi.org/10.3389/frwa.2023.1278205

Preisser, M., Passalacqua, P., Bixler, R. P., & Hofmann, J. (2022). Intersecting near-real time fluvial and pluvial inundation estimates with sociodemographic vulnerability to quantify a household flood impact index. *Hydrology and Earth System Sciences*, *26*(15), 3941–3964. https://doi.org/10.5194/hess-26-3941-2022

Ridder, N. N., Pitman, A. J., Westra, S., Ukkola, A., Do, H. X., Bador, M., et al. (2020). Global hotspots for the occurrence of compound events. *Nature Communications*, *11*(1), 5956. https://doi.org/10.1038/s41467-020-19639-3

Rogers, C., ad Sara Perkins-Kirkpatrick, K. K., Loikith, P., & Singh, D. (2022). Sixfold increase in historical northern hemisphere concurrent large heatwaves driven by warming and changing atmospheric circulations. *Journal of Climate*, *35*(3), 1063–1078. https://doi.org/10.1175/jcli-d-21-0200.1

Rogers, C. D. W., Ting, M., Li, C., Kornhuber, K., Coffel, E. D., Horton, R. M., et al. (2021). Recent increases in exposure to extreme humid-heat events disproportionately affect populated regions. *Geophysical Research Letters*, *48*(19), e2021GL094183. https://doi.org/10.1029/2021gl094183

Rufat, S., Tate, E., Burton, C. G., & Maroof, A. S. (2015). Social vulnerability to floods: Review of case studies and implications for measurement. *International Journal of Disaster Risk Reduction*, *14*, 470–486. https://doi.org/10.1016/j.ijdrr.2015.09.013

Saharia, M., Jain, A., Baishya, R. R., Haobam, S., Sreejith, O. P., Pai, D. S., & Rafieeinasab, A. (2021). India flood inventory: Creation of a multi-source national geospatial database to facilitate comprehensive flood research. *Natural Hazards*, *108*(1), 619–633. https://doi.org/10.1007/s11069-021-04698-6

Salvo, C., & Vitale, A. (2023). A remote sensing method to assess the future multi-hazard exposure of urban areas. *Remote Sensing*, *15*(17), 4288. https://doi.org/10.3390/rs15174288

Sanders, B. F., Schubert, J. E., Kahl, D. T., Mach, K. J., Brady, D., AghaKouchak, A., et al. (2022). Large and inequitable flood risks in Los Angeles, California. *Nature Sustainability*, *6*(1), 47–57. https://doi.org/10.1038/s41893-022-00977-7

Schubert, J. E., Mach, K. J., & Sanders, B. F. (2024). National-scale flood hazard data unfit for urban risk management. *Earth's Future*, *12*(7). https://doi.org/10.1029/2024ef004549

Schumann, G. J.-P., Frye, S., Wells, G., Adler, R., Brakenridge, R., Bolten, J., et al. (2016). Unlocking the full potential of Earth observation during the 2015 Texas flood disaster. *Water Resources Research*, *52*(5), 3288–3293. https://doi.org/10.1002/2015wr018428

Seong, K., Jiao, J., & Mandalapu, A. (2022). Evaluating the effects of heat vulnerability on heat-related emergency medical service incidents: Lessons from Austin, Texas. *Environment and Planning B: Urban Analytics and City Science*, *50*(3), 776–795. https://doi.org/10.1177/23998083221129618

Shayegh, S., Manoussi, V., & Dasgupta, S. (2020). Climate change and development in South Africa: The impact of rising temperatures on economic productivity and labour availability. *Climate & Development*, *13*(8), 725–735. https://doi.org/10.1080/17565529.2020.1857675

Shi, P., Yang, X., Liu, F., Li, M., Pan, H., Yang, W., et al. (2015). Mapping multi-hazard risk of the world. In *World atlas of natural disaster risk* (pp. 287–306). Springer Berlin Heidelberg. https://doi.org/10.1007/978-3-662-45430-5_16

Smale, D. A., Wernberg, T., Oliver, E. C. J., Thomsen, M., Harvey, B. P., Straub, S. C., et al. (2019). Marine heatwaves threaten global biodiversity and the provision of ecosystem services. *Nature Climate Change*, *9*(4), 306–312. https://doi.org/10.1038/s41558-019-0412-1

Stalhandske, Z., Steinmann, C. B., Meiler, S., Sauer, I. J., Vogt, T., Bresch, D. N., & Kropf, C. M. (2024). Global multi-hazard risk assessment in a changing climate. *Scientific Reports*, *14*(1), 5875. https://doi.org/10.1038/s41598-024-55775-2

Sutanto, S. J., Vitolo, C., Di Napoli, C., D'Andrea, M., & Van Lanen, H. A. (2020). Heatwaves, droughts, and fires: Exploring compound and cascading dry hazards at the pan-European scale. *Environment International*, *134*, 105276. https://doi.org/10.1016/j.envint.2019.105276

Tellman, B., Sullivan, J. A., Kuhn, C., Kettner, A., Doyle, C. S., Brakenridge, R., et al. (2021). Satellite imaging reveals increased proportion of population exposed to floods. *Nature*, *596*(7870), 80–86. https://doi.org/10.1038/s41586-021-03695-w

Tilloy, A., Malamud, B. D., Winter, H., & Joly-Laugel, A. (2019). A review of quantification methodologies for multi-hazard interrelationships. *Earth-Science Reviews*, *196*, 102881. https://doi.org/10.1016/j.earscirev.2019.102881

TWDB. (2024). State flood plan (techreport). *Texas Water Development Board*. Retrieved from https://www.twdb.texas.gov/flood/planning/sfp/doc/Draft2024StateFloodPlan_VolumeI.pdf

UNDRR. (2016). *Report of the open-ended intergovernmental expert working group on indicators and terminology relating to disaster risk reduction (resreport No. 21184)*. United Nations.

Wang, J., He, Z., & Weng, W. (2020). A review of the research into the relations between hazards in multi-hazard risk analysis. *Natural Hazards*, *104*(3), 2003–2026. https://doi.org/10.1007/s11069-020-04259-3

Ward, P. J., Daniell, J., Duncan, M., Dunne, A., Hananel, C., Hochrainer-Stigler, S., et al. (2022). Invited perspectives: A research agenda towards disaster risk management pathways in multi-(hazard-)risk assessment. *Natural Hazards and Earth System Sciences*, *22*(4), 1487–1497. https://doi.org/10.5194/nhess-22-1487-2022

Ward, P. J., Jongman, B., Salamon, P., Simpson, A., Bates, P., De Groeve, T., et al. (2015). Usefulness and limitations of global flood risk models. *Nature Climate Change*, *5*(8), 712–715. https://doi.org/10.1038/nclimate2742

Winsemius, H. C., Aerts, J., van Beek, L., Bierkens, M., Bouwman, A., Jongman, B., et al. (2015). Global drivers of Future River flood risk. *Nature Climate Change*, *6*(4), 381–385. https://doi.org/10.1038/nclimate2893

Wu, H., Adler, R. F., Hong, Y., Tian, Y., & Policelli, F. (2012). Evaluation of global flood detection using satellite-based rainfall and a hydrologic model. *Journal of Hydrometeorology*, *13*(4), 1268–1284. https://doi.org/10.1175/jhm-d-11-087.1

Wu, H., Adler, R. F., Tian, Y., Huffman, G. J., Li, H., & Wang, J. (2014). Real-time global flood estimation using satellite-based precipitation and a coupled land surface and routing model. *Water Resources Research*, *50*(3), 2693–2717. https://doi.org/10.1002/2013wr014710

Zhang, T., Zhou, Y., Zhao, K., Zhu, Z., Chen, G., Hu, J., & Wang, L. (2022). A global dataset of daily maximum and minimum near-surface air temperature at 1 km resolution over land. *Earth System Science Data*, *14*(12), 5637–5649. https://doi.org/10.5194/essd-14-5637-2022

Zhang, W., Liu, Y., Tang, W., Wang, W., & Liu, Z. (2022). Assessment of the effects of natural and anthropogenic drivers on extreme flood events in coastal regions. *Stochastic Environmental Research and Risk Assessment*, *37*(2), 697–715. https://doi.org/10.1007/s00477-022-02306-y

Zhang, W., & Villarini, G. (2020). Deadly compound heat stress-flooding hazard across the central United States. *Geophysical Research Letters*, *47*(15), e2020GL089185. https://doi.org/10.1029/2020gl089185

Zheng, F., Westra, S., & Sisson, S. A. (2013). Quantifying the dependence between extreme rainfall and storm surge in the coastal zone. *Journal of Hydrology*, *505*, 172–187. https://doi.org/10.1016/j.jhydrol.2013.09.054

Zscheischler, J., Martius, O., Westra, S., Bevacqua, E., Raymond, C., Horton, R. M., et al. (2020). A typology of compound weather and climate events. *Nature Reviews Earth & Environment*, *1*(7), 333–347. https://doi.org/10.1038/s43017-020-0060-z